

## Anti-corrosive Properties and Quantum Chemical Study of (E)-4-Methoxy-N-(Methoxybenzylidene)Aniline and (E)-N-(4-Methoxybenzylidene)-4-Nitroaniline Coating on Mild Steel in Molar Hydrochloric.

H. Elmsellem<sup>1</sup>, H. Nacer<sup>2</sup>, F. Halaimia<sup>1</sup>, A. Aouniti<sup>1</sup>, I. Lakehal<sup>3</sup>, A. Chetouani<sup>1,4</sup>, S. S. Al-Deyab<sup>5</sup>, I. Warad<sup>6</sup>, R. Touzani<sup>1</sup>, B. Hammouti<sup>1,5,\*</sup>

<sup>1</sup>Laboratory of Applied Chemistry and Environment (LCAE-URAC18), Faculté des Sciences, Université Mohammed Premier, B.P. 717, M-60000 Oujda, Morocco

<sup>2</sup>Université Larbi ben M'Hidi d'Oum-EL-Bouaghi. Oum-EL-Bouaghi 4000. Algérie

<sup>3</sup>Laboratoire de synthèse organique et modélisation. Université Badji mokhtar. Annaba. BP12 El-Hadjar. Annaba 23000. Algérie

<sup>4</sup>Laboratoire de chimie physique, Centre Régionale des Métiers de l'Education et de Formation "CRMEF", Région de l'Orientale, M-60000 Oujda, Morocco.

<sup>5</sup>Department of Chemistry, College of Science, King Saud University, B.O. 2455, Riyadh 11451, Saudi Arabia

<sup>6</sup>Department of Chemistry, AN-Najah National University, Nablus, Palestine

\*E-mail: [hammoutib@gmail.com](mailto:hammoutib@gmail.com)

Received: 28 May 2013 / Accepted: 19 May 2014 / Published: 16 June 2014

---

The effect of (E)-4-methoxy-N-(methoxybenzylidene)aniline (P1) and (E)-N-(4-methoxybenzylidene)-4-nitroaniline (P2) on the corrosion of steel in molar hydrochloric acid studied by weight loss and electrochemical polarisation. The results obtained reveal that the compounds reduce the corrosion rate. The inhibition efficiency increases with the increase of inhibitor concentration. Potentiodynamic polarisation studies clearly reveal that the presence of the inhibitors does not change the mechanism of the hydrogen evolution reaction and acts essentially as mixed inhibitors. We note good agreement between gravimetric and electrochemical methods. The influence of temperature and inhibitor concentration on the corrosion of mild steel has also been investigated in the temperature range 308 - 353K, indicates that inhibition efficiency remains almost constant with temperature. The adsorption of the inhibitors on the mild steel surface in both acids obeys the Langmuir' adsorption isotherm. The thermodynamic parameters of adsorption deduced reveal a strong interaction and spontaneous adsorption of P1 and P2 on the mild steel surface. Also the objective of this work is to attempt to find relationships between their molecular and electronic structures and inhibition efficiency. The structural parameters, such as the frontier molecular orbital energies ( $E_{HOMO}$  and  $E_{LUMO}$ ), gap of energy  $\Delta E$ , the charge distribution, the absolute hardness  $\eta$  and the softness  $\sigma$ , the fraction of electrons  $\Delta N$  transferred from the molecules to iron as well as electronic parameters such as Mulliken atomic populations and Fukui indices were calculated and discussed.

---

**Keywords:** steel, imines, aniline, inhibition, corrosion, acid, Quantum chemical, DFT.

## 1. INTRODUCTION

Mild steel is an industrially important structural material and is corroded by many agents, of which aqueous acids are the most dangerous. The protection of steel from corrosion is the need of an hour. Already, substituted thiourea derivatives have been proved to be fairly effective in corrosion control.

Corrosion in general terminology is the destructive attack of metal. Metals are exposed to action of acids in many different ways and for many reasons. Metal loss or damage can occur due to chemical & electrochemical reaction, physical erosion or biological attack. Corrosion is always because of chemical reaction. Water corrosiveness is determined by the impurities present in it. Oxygen, dissolved solids, gases and acids in water attack the common construction material. The exposures can be most severe but in many cases, the corrosion can be controlled by means of inhibitors. A considerable amount of interest has been generated in the study of organic inhibitors owing to their usefulness in several industries: during the pickling of metals, cleaning of boilers, oil and gas wells acidizing, acid decaling [1, 2].

The importance of inhibitive protection in acidic solutions is increased by the fact that iron materials which are more susceptible to be attacked in aggressive media, are the commonly exposed metals in industrial environments. The corrosion inhibitors act in a number of ways to retard or delay the corrosion mechanism: in simple terms, they form a chemical inhibition film on the steel reinforcement at either the anode and/or cathode. There are two key types of corrosion inhibitor to choose from: organic and inorganic. The effect of organic nitrogen compounds on the corrosion behaviour of iron and steel in acidic solutions has been reported [3].

It's shown that the protective properties of such compounds depended upon their ability to reduce corrosion rate and enhanced at higher electron densities around the nitrogen atoms. In addition, some molecular geometry properties of the inhibitors can also play a determined role in the enhancement of their corrosion inhibition efficiencies, such as the planarity of the system, the molecular size and the presence of multiple adsorption active centers with lone pair and/or orbitals whose electronic density is higher at the donor atom. Therefore, the choice of effective inhibitors is usually based on their structure, their mechanism of action and their electron donating ability mixed corrosion inhibitors have been also used because of their many important characteristics. The effectiveness of heterocyclic molecules as corrosion inhibitors is based on their chelating action and the formation of an insoluble physical diffusion barrier on the electrode surface, preventing metal reaction and dissolution. Such a barrier is readily formed by nitrogen – containing heterocyclic molecules due to the strong  $\pi$ -interaction between the aromatic rings. Their high inhibition efficiencies were attributed to the strong adsorption on the metal surface through their N heteroatom [1, 4].

It has been shown that organic compounds are containing both nitrogen and oxygen atoms are of particular interest as they give better inhibition efficiencies than those containing nitrogen or oxygen alone. These are polar molecules with nitrogen atom having a permanent negative charge whereas the oxygen atom has a positive charge. As the molecule approaches the electrode surface, the electric field of double layer increases the polarization of molecules and induces additional charges on nitrogen and oxygen atoms, a condition that enhances the adsorption of molecules. Furthermore, former studies

concluded that the adsorption on the metal surface depends on the availability of non-bonded lone-pair and  $\pi$  electrons in inhibitor molecules which facilitate electron transfer from the inhibitor to the metal and allow the formation of covalent bond between the inhibitor and the metal surface [5, 6].

The present paper reports the study of the inhibitive action of the (E)-4-methoxy-N-(methoxybenzylidene)aniline (P1) and (E)-N-(4-methoxybenzylidene)-4-nitroaniline (P2) on the corrosion of steel in molar hydrochloric acid. The corrosion behaviour of steel has been evaluated by weight loss and potentiodynamic polarisation and EIS measurements. The molecular structures of these compounds are presented in Fig.1. This work was to investigate computationally, in gas and aqueous phases, using DFT at B3LYP/6-31G\*\* level of theory, four newly synthesized imine derivatives denoted hereafter P1 and P2 as shown in Fig. 1. In the following, we attempt to find good theoretical parameters to characterize, the inhibition properties of the inhibitors under study and the correlation between the inhibition efficiency and the electronic as well as geometric properties of these molecules.

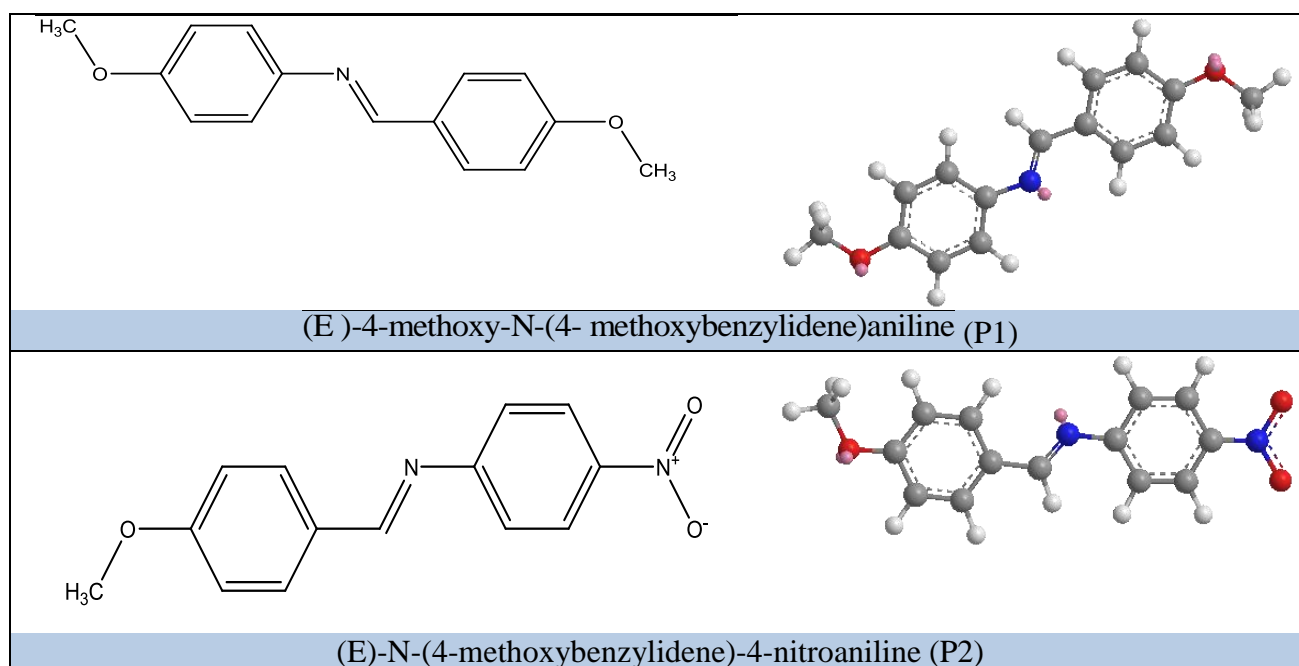


**Figure 1.** Molecular structure of P1 and P2

## 2. EXPERIMENTAL DETAILS

### 2.1. Chemistry

All new compounds were synthesized and characterized by  $^1\text{H}$  NMR,  $^{13}\text{C}$  NMR, IR, and LCMS.  $^1\text{H}$  NMR (400 MHz) and  $^{13}\text{C}$  NMR (100 MHz) spectra were measured in DMSO at room temperature. The synthesis characterisation and theoretical studies of the new ligands based on aniline will be the subject of a future publication, named by our researchers include I. Lakehal, F. Abridach, F. Halaimia, H. Nacer, B. Hammouti, R. Touzani.

The molecular inhibitors P1 and P2 were minimised by MM2 method. The MM2 force field method is available of ChemBio3D. MM2 is most commonly used for calculating properties of organic

molecular models. The MM2 procedures described assume that you understand how the potential energy surface relates to conformations of your model. In ChemBio3D 12.0, the MM2 atom type is used for force field calculations and used only in building models were shows in Fig 1. Table 1 brings together the different parameters to calculate from the MM2 method, such as. Stretch, Bend, Stretch-Bend, Torsion, Non-1,4 VDW, 1,4 VDW Dipole/Dipole and Total Energy.

**Table 1.** Parameters Minimize Energy Computation of P1 and P2

	P1	P2
Stretch	0.9507	0.7603
Bend	6.9915	4.9802
Stretch-Bend	0.2059	0.1652
Torsion	-13.3213	-13.3060
Non-1,4 VDW	0.7102	0.7996
1,4 VDW	13.5538	11.8797
Dipole/Dipole	0.0139	0.3507
Total Energy ( kcal/mol)	9.1047	5.9250

## 2.2. Material preparation

Corrosion tests have been carried out on electrodes cut from sheets of mild steel. The experiments were performed with mild steel with the following composition table 2. Samples were polished with emery paper up to 1200 grade, and then washed with double-distilled water, and degreased with ethanol and dried at room temperature before use. The solutions (1M HCl) were prepared by dilution of an analytical reagent grade 37% HCl with doubly distilled water.

**Table 2.** Chemical composition of mild steel.

Elements	Fe	P	Si	Al	Mn	C	S
% en masse	99.21	0.09	0.38	0.01	0.05	0.21	0.05

## 2.3. Gravimetric measurements

For weight loss measurements, each run was carried out in a double walled glass cell equipped with a thermostat-cooling condenser containing 100 ml test solution. The steel specimens used had a rectangular form (1.5 × 1.5 × 0.05 cm), was completely immersed at inclined position in the vessel. The immersion time for the weight loss was 6h at 308K. After 6 h of immersion, the electrode was withdrawn, rinsed with doubly distilled water, washed with ethanol, dried and weighed. Duplicate experiments were performed in each case and the mean value of the weight loss has been reported. The weight loss was used to calculate the corrosion rate ( $W$ ) in milligrams per square centimetre per hour ( $\text{mg}/\text{cm}^2 \text{ h}$ ).

From the weight loss results, the corrosion rate (CR), the inhibition efficiency ( $\eta_{WL}(\%)$ ) of the inhibitor and degree of surface coverage ( $\theta$ ) were calculated using equations 4, 5 and 6;

$$C_R = \frac{W_b - W_a}{At} \quad (1)$$

$$\eta_{WL}(\%) = \left(1 - \frac{w_i}{w_0}\right) \times 100 \quad (2)$$

$$\theta = 1 - \frac{w_i}{w_0} \quad (3)$$

where  $W_b$  and  $W_a$  are the specimen weight before and after immersion in the tested solution,  $w_0$  and  $w_i$  are the values of corrosion weight losses of carbon steel in uninhibited and inhibited solutions, respectively,  $A$  the total area of the carbon steel specimen ( $\text{cm}^2$ ) and  $t$  is the exposure time (h) and  $\theta$  is the degree of surface coverage of the inhibitor.

#### 2.4. Electrochemical measurements.

Electrochemical measurements were conducted in a conventional three-electrode thermostated cell. A platinum disc was used as counter electrode and a saturated calomel electrode (SCE) as reference electrode. The working electrode was an ordinary steel disc. The specimens were machined into cylinders and mounted in polytetrafluoroethylene (PTFE) moulds. The area in contact with the corrosive solution was  $1 \text{ cm}^2$ . The working electrode was immersed in the test solution during 1 h until a steady-state open circuit potential ( $E_{ocp}$ ) was obtained. The cell was thermostated at 308K.

The polarisation curves realised with scan rate of  $1 \text{ mV/min}$ . Before recording the cathodic potentiokinetic curves up the corrosion potential, the iron electrode was polarised at  $800 \text{ mV/SCE}$  for 10min. However, for anodic polarisation curves, the potential of the working electrode was swept from its open circuit potential value after 30 min at rest. After this scan, the anodic polarization curve was recorded by polarization from the  $E_{ocp}$  to positive direction.

For electrochemical impedance spectroscopy (EIS) measurements and after the determination of steady-state current at a given potential, sine wave voltage ( $10 \text{ mV}$ ) peak to peak, at frequencies between  $100 \text{ kHz}$  and  $10 \text{ MHz}$  were superimposed on the rest potential. Computer programs automatically controlled the measurements performed at rest potentials after 30 min of exposure. The impedance diagrams are given in the Nyquist representation. The potentiodynamic measurements were carried out using a Potentiostat type, VoltaLab PGZ 100, controlled by a personal computer. Since the conductivity of medium studied is low, the polarization curves  $J(E)$  were corrected from ohmic drop; that is, by  $R_s \times J$ . The solution resistance,  $R_s$ , was determined by the electrochemical impedance spectroscopy. On the Nyquist diagrams,  $R_s$  is the abscissa of high-frequency intersection of the diagram with the real axis .

The evaluation of corrosion kinetics parameters was obtained using a fitting by Stern–Geary equation. The inhibition efficiency was evaluated from the measured  $J_{corr}$  values using the relationship:

$$IE\% = \left(1 - \frac{j_{corr}}{j_{corr}^0}\right) \times 100 \quad (4)$$

The degree of surface coverage ( $\theta$ ) and the inhibition efficiency IE% were calculated from the following equations:

$$\theta = 1 - \frac{j_{corr}}{j_{corr}^0} \quad (5)$$

Where  $j_{corr}^0$  and  $j_{corr}$  are the corrosion current values without and with the addition of various concentration of inhibitor.

The inhibiting properties of the tested compounds have also been also evaluated by the determination of the polarisation resistance. The corresponding polarisation resistance ( $R_p$ ) values of steel in 1M HCl in the absence of different concentration of the inhibitor. The inhibition efficiency ( $E_{Rp}$ ) was defined as follow equation, where  $R'_p$  and  $R_p$  are the polarisation resistance in presence and in absence of the inhibitor, respectively [7].

$$E_{Rp} = \left(1 - \frac{R_p}{R'_p}\right) \cdot 100 \quad (6)$$

## 2.5. Theoretical methodology.

The geometries of the studied compounds have been fully optimized at Density Functional Theory (Becke's Three Parameter Hybrid Functional using the Lee, Yang and Parr Correlation Functional B3LYP [8-10] . The basis set 6-31G (d) was used for all atoms. The quantum chemical calculations using standard Gaussian-03 software package with complete geometry optimizations without constrains. Indeed, DFT methods are often the methods of choice for similar calculations because of their ability to overcome one of the main disadvantages of ab-initio methods; the complete neglect of electron correlation; by including some of it at greatly reduced computational cost. Thus, all the parameters presented in this work were calculated at B3LYP with 6-31G\*\* basis set, frequently used for similar molecules [11, 12].

These methods model the solvent as a continuum of uniform dielectric constant ( $\epsilon$ ) and define the cavity where the solute is placed as a uniform series of interlocking atomic spheres. Since we cannot represent the implicit effect of hydrogen chloride solution, water is instead used to include the solvent effect ( $\epsilon = 78.5$ ) [8].

The aim of this work is to investigate whether there is a clear relationship between the experimentally determined inhibition efficiencies of the studied inhibitors and a number of quantum-chemical parameters. Some of these parameters are directly extracted from the output files ( $E_{HOMO}$ ,  $E_{LUMO}$ ,  $\mu$ ) when other parameters needs to be computed separately ( $IP$ ,  $EA$ ,  $\Delta E$ ,  $\chi$ ,  $\eta$ ,  $\sigma$  and  $\Delta N$ ).

For closed-shell molecules, ionization potential  $IP$  and electron affinity  $EA$  can be expressed as follows in terms of  $E_{HOMO}$ ,  $E_{LUMO}$  the highest occupied molecular orbital energy, and the lowest unoccupied molecular orbital energy, respectively:

$$IP = -E_{HOMO} \quad (7)$$

$$EA = -E_{LUMO} \quad (8)$$

When the values of  $IP$  and  $EA$  are known, one can determine through the following expressions the values of the absolute electronegativity  $\chi$ , the absolute hardness  $\eta$  and the softness  $\sigma$  (the inverse of the hardness):

$$\chi = \frac{IP + EA}{2} \quad (3)$$

$$\eta = \frac{IP - EA}{2} \quad (9)$$

$$\sigma = \frac{1}{\eta} \quad (10)$$

Moreover, for a reaction of two systems with different electronegativities the electronic flow will occur from the molecule with the lower electronegativity (the organic inhibitor) towards that of higher value (metallic surface), until the chemical potentials are equal [13]. Therefore the fraction of electrons transferred ( $\Delta N$ ) from the inhibitor molecule to the metallic atom was calculated according to Pearson electronegativity scale [14-16] :

$$\Delta N = \frac{\chi_{Fe} - \chi_{inh}}{2(\eta_{Fe} + \eta_{inh})} \quad (11)$$

Where  $\chi_{Fe}$  and  $\chi_{inh}$  denote the absolute electronegativity of *Fe* and the inhibitor molecule, respectively;  $\eta_{Fe}$  and  $\eta_{inh}$  denote the absolute hardness of *Fe* and the inhibitor molecule, respectively. A theoretical value for the electronegativity of bulk iron was used  $\chi_{Fe} = 7$  eV and a global hardness of  $\eta_{Fe} = 0$ , by assuming that for a metallic bulk  $IP = EA$  because they are softer than the neutral metallic atoms. The natural bond orbital analysis allowed us to describe the bonding in terms of the natural hybrids centered on each atom. The population analysis has been performed on the neutral, cationic and anionic species at the same obtained optimized geometry of each inhibitor in order to determine their Fukui Functions.

### 3. RESULTS AND DISCUSSION

Weight loss of C-steel, in  $\text{mg.cm}^{-2}$  of the surface area, was determined at different concentration in the absence and presence of (E)-4-methoxy-N-(methoxybenzylidene)aniline (P1) and (E)-N-(4-methoxybenzylidene)-4-nitroaniline (P2) in 1M HCl after 6 h at 308 K. The values of  $\eta_{WL}(\%)$  for two inhibitors are given in Table 3.

Results obtained show that the inhibition efficiency increases with the increasing inhibitor concentration. These results reveal that the compounds under investigation are fairly efficient inhibitors for C-steel dissolution in 1M HCl solution. The results show that corrosion rates decrease with increase of (P1) and (P2). In the presence of P1 and P2 at  $2.0 \cdot 10^{-3}\text{M}$ , the corrosion rate is observed to reduce significantly and we can conclude that the compounds have the best inhibitory efficiencies in the three corrosive environments. The inhibition efficiency is found to increase with increasing concentration of P1 and P2 up to  $2.0 \cdot 10^{-3}\text{M}$  to attain 95% and 60%, respectively.

The inhibition of corrosion of C-steel by P1, specially, can be explained in terms of adsorption on the metal surface [4, 17] . These compounds can be absorbed by the interaction between lone pairs of electrons of nitrogen atoms of the inhibitors and the metal surface. This process is facilitated by the presence of vacant orbital of low energy in iron atom, as observed in the transition group elements. Careful inspection of these results showed that, the ranking of the inhibitors according to  $\eta_{WL}(\%)$  is as follows: P1 > P2 for the same concentration

**Table 3.** Gravimetric results of steel in acid at different concentrations of P1, and P2 at 6h and 308 K

Inhibitors	Conc (M)	$10^{-4} \times CR$ (mg cm <sup>-2</sup> h <sup>-1</sup> )	$\eta_{WL}(\%)$	$\theta$
HCl	1	0,82	---	--
P1	$10^{-6}$	0,54	34.23	0.34
	$5 \cdot 10^{-6}$	0,50	38.68	0.39
	$10^{-5}$	0,43	47.43	0.47
	$5 \cdot 10^{-5}$	0,37	54.62	0.55
	$10^{-4}$	0,28	66.36	0.66
	$5 \cdot 10^{-4}$	0,25	70.03	0.70
	$10^{-3}$	0,09	89.02	0.89
	$2 \cdot 10^{-3}$	0,04	95.12	0.95
P2	$10^{-6}$	0,50	21.58	0.22
	$5 \cdot 10^{-6}$	0,47	24.19	0.24
	$10^{-5}$	0,42	30.91	0.31
	$5 \cdot 10^{-5}$	0,35	39.86	0.40
	$10^{-4}$	0,32	43.42	0.43
	$5 \cdot 10^{-4}$	0,28	47.99	0.48
	$10^{-3}$	0,27	49.24	0.49
	$2 \cdot 10^{-3}$	0,18	59.70	0.60

### 3.1. Effect of temperature

In general, corrosion rates increase with increasing temperature. In seawater, this increase is much less than the doubling of reaction rates with each 18°F rise in temperature that would be expected if the reactions were under diffusion control as are many other chemical reactions. For many materials, such as steels, where the oxygen content of the water directly affects the corrosion rate, the effect of temperature is minimal as in situations where the corrosion rate would be increased by increased temperature, the solubility of oxygen is decreased with increasing temperatures and the two effects counteract each other. Steels and iron alloys are particularly insensitive to temperature effects in normal marine immersion. For other alloys that depend on a passive film for their corrosion resistance, the effects of temperature can be more pronounced. At elevated temperatures the solubility oxygen required for repairing protective oxide films found on many passive materials is reduced and the reactions that cause the films to break down are enhanced by the increased temperatures. Many stainless steels have what is essentially a “critical pitting temperature” in seawater that is in the range of temperatures experienced in natural seawater. In cold waters they do not pit but in warmer waters they are susceptible.

For most chemical reactions, the reaction rate increases with increasing temperature. Temperature affects the corrosion rate of metals in electrolytes primarily through its effect on factors which control the diffusion rate of oxygen. The corrosion of iron and steel is an example of this because temperature affects the corrosion rate by virtue of its effect on the oxygen solubility and oxygen diffusion coefficient. As temperature increases the diffusion coefficient of oxygen also increases which tends to increase the corrosion rate. However as temperature is increased oxygen solubility in aqueous solutions decreases until at the boiling point all oxygen is removed; this factor

tends to decrease the corrosion rate. The net affect fo mild steel, is that the corrosion rate approximately doubles for a temperature rise of 313K up to a maximum temperature at about 343, the rate then falls off in an open system because the decreall in oxyben solubility becomes the most important factor. In a closed system, where oxygen cannot escape the corrosion rate continues to increase indefinitely with temperature until all the oxygen is consumed (Source: "Corrosion Control" NAVFAC MO-307 september 1992.)

The effect of temperature on the inhibited acid–metal reaction is highly complex because many changes occur on the metal surface, such as rapid etching and desorption of the inhibitor and the inhibitor itself, in some cases, may undergo decomposition and/or rearrangement. However, it provides the ability of calculating many thermodynamic functions for the inhibition and/or the adsorption processes which contribute in determining the type of adsorption of the studied inhibitors [18] .

We have studied the temperature influence on the efficiency of (E)-4-methoxy-N-(methoxybenzylidene)aniline (P1). For this purpose, we made weight-loss measurements in the range of temperature 3013-343 K, in the presence and absence of oil at various concentrations during 1h of immersion. The corresponding data are shown in Table 4. We remark that the rise in temperature leads to an increase in corrosive rate with and without inhibitor. We also note the increase in the inhibition efficiency of P1 with temperature.

**Table 4.** The effect of P1 concentration on the weight loss of steel/HCl and efficiency at different temperatures.

T (K)	Concentration (M)	W(mg.cm <sup>-2</sup> h <sup>-1</sup> )	$\theta$	E (%)
313	0	1.69	--	--
	5. 10 <sup>-5</sup>	0.9	0.47	46.75
	10 <sup>-4</sup>	0.58	0.66	65.68
	5. 10 <sup>-4</sup>	0.24	0.86	85.80
	10 <sup>-3</sup>	0.15	0.91	91.12
	2 .10 <sup>-3</sup>	0.09	0.95	94.67
323	0	3.23	--	--
	5. 10 <sup>-5</sup>	2.01	0.38	37.77
	10 <sup>-4</sup>	1.46	0.55	54.80
	5. 10 <sup>-4</sup>	0.62	0.81	80.80
	10 <sup>-3</sup>	0.45	0.86	86.07
	2 .10 <sup>-3</sup>	0.29	0.91	91.02
333	0	6.73	--	--
	5. 10 <sup>-5</sup>	4.13	0.39	38.63
	10 <sup>-4</sup>	3.46	0.49	48.59
	5. 10 <sup>-4</sup>	1.72	0.74	74.44
	10 <sup>-3</sup>	1.15	0.83	82.91
	2 .10 <sup>-3</sup>	0.84	0.88	87.52
343	0	10.39	--	--
	5. 10 <sup>-5</sup>	6.77	0.35	34.84
	10 <sup>-4</sup>	5.35	0.49	48.51
	5. 10 <sup>-4</sup>	3.44	0.67	66.89
	10 <sup>-3</sup>	2.43	0.77	76.61
	2 .10 <sup>-3</sup>	1.84	0.82	82.29

The corresponding results are given in Table 5. The activation energies for the corrosion process were calculated from the Arrhenius equation (7):

$$W = A \exp\left(-\frac{E_a}{RT}\right) \quad (12)$$

where  $E_a$  represents the apparent activation energy,  $R$  the gas constant,  $T$  the absolute temperature,  $A$  the pre-exponential factor and  $W$  the corrosion rate, obtained from the weight loss method. Literature discussed the variation of the apparent activation energy  $E_a$  in the presence and absence of inhibitor. Higher values for  $E_a$  were found in the presence of inhibitors and showed that in the presence of inhibitor the apparent activation energy was lower than that in the absence of inhibitor [19, 20].

However, in our study,  $E_a$  increases with increasing the P1 concentration, and all values of  $E_a$  were higher than that in the absence of this inhibitor. This type of inhibitor retards corrosion at ordinary temperatures but inhibition is diminished at elevated temperature. It is clear also, that the increase of corrosion rate is more pronounced with the rise of temperature for the blank solution. In the presence of the tested molecules,  $W_{\text{corr}}$  is reduced even at high temperature.  $E$  (%) passed from 94.67 to 82.29% for P1, when temperature rises from 313 to 343 K at  $2.0 \cdot 10^{-3}$  M. We note that the efficiency of the inhibitors tested depends on the temperature and decreases with the rise of temperature from 313 to 343 K.

Arrhenius law predicts that corrosion rate increases with the temperature and  $E_a$  and  $A$  may vary with temperature (Eq. 1). The obtained values seem that  $A$  and  $E_a$  increase continuously with the inhibitor's concentration. Other kinetic data (enthalpy and entropy of corrosion process) are accessible using the alternative formulation of Arrhenius equation [15]:

$$W = \frac{RT}{Nh} \exp\left(\frac{\Delta S_a^\circ}{R}\right) \exp\left(-\frac{\Delta H_a^\circ}{RT}\right) \quad (13)$$

where  $h$  is plank's constant,  $N$  is Avogadro's number,  $\Delta S_a^\circ$  and  $\Delta H_a^\circ$  are the entropy and enthalpy of activation, respectively. Plots of  $\ln(W/T)$  vs. the reciprocal of temperature show straight lines with a slope equal to  $(-\Delta H_a^\circ/R)$  and an intercept of  $(\ln R/Nh + \Delta S_a^\circ/R)$ . The values of  $\Delta H_a^\circ$  and  $\Delta S_a^\circ$  are also presented in Table 5.

Inspection of the kinetic data obtained in Table 5 shows that all parameters of corrosion process increases with the inhibitor concentration. Literature postulates that the positive sign of the enthalpy ( $\Delta H_a^\circ$ ) is an endothermic nature of the steel dissolution process. The entropy of activation  $\Delta S_a^\circ$  in the absence of inhibitors is positive and this value increases positively with the P1 concentration. The increase of  $\Delta S_a^\circ$  implies that an increase in disordering takes place on going from reactants to the activated complex [17].

The increase of  $E_a$  and  $\Delta H_a^\circ$  with an increase in the P1 concentration (Fig. 2) suggests that the energy barrier of corrosion reaction increases with the inhibitor's concentration. The higher activation energy in the inhibitor's presence further supports the proposed physisorption mechanism. Unchanged or lower values of  $E_a$  in inhibited systems compared to the blank to be indicative of chemisorption mechanism, while higher values of  $E_a$  suggest a physical adsorption mechanism [21]. This type of inhibitors retards the corrosion process. It is also interested to verify the known thermodynamic relation between  $E_a$  and  $\Delta H_a^\circ$ :

$$E_a - \Delta H_a^\circ = RT \quad (14)$$

The calculate values are too close to RT is 2.68 kJ/mol. This result shows the inhibitor acted equally on  $E_a$  and  $\Delta H_a^\circ$ .

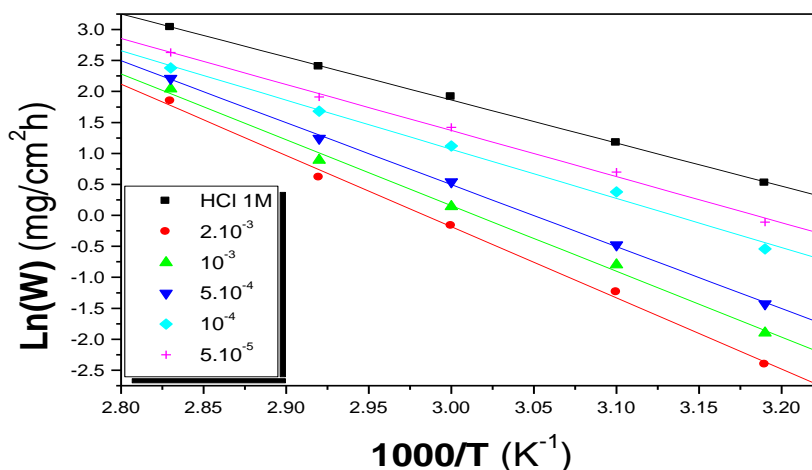


Figure 2. Arrhenius plots of steel in acid with and without different P1 concentrations

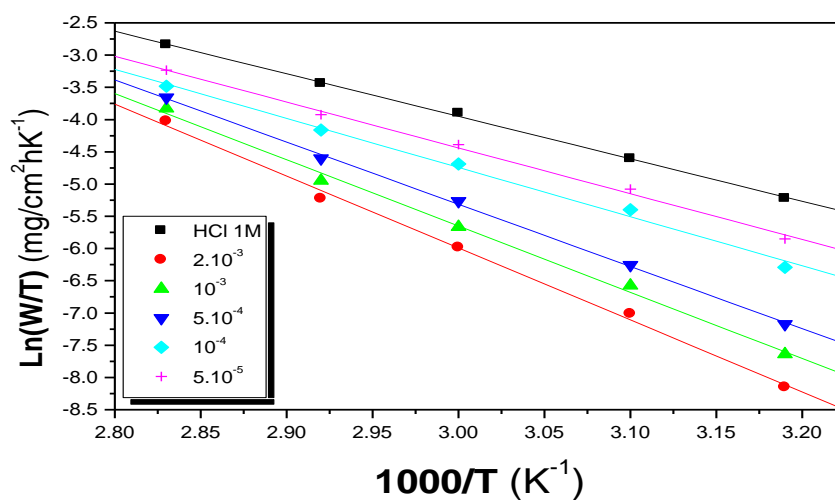


Figure 3. The relation between Ln (W/T) and 1/T for different P1 concentrations

Table 5. Kinetic parameters of activation as function of inhibitor concentration of P1

Concentration	Linear Coefficient	$E_a$ (kJ/mol)	$\Delta H_a^\circ$ (kJ/mol)	$E_a - \Delta H_a^\circ$	$\Delta S_a^\circ$ (J/mol.K)
Blank	1.000	57.76	54.79	2.97	-65.88
$5.10^{-5}$	0.998	61.82	59.06	2.76	-57.15
$10^{-4}$	0.997	65.98	63.36	2.62	-46.79
$5.10^{-4}$	1.000	83.15	80.21	2.94	-0.98
$10^{-3}$	0.998	88.34	85.43	2.91	11.89
$2.10^{-3}$	0.999	95.58	92.78	2.80	31.10

### 3.2. Thermodynamic parameters and adsorption isotherm.

Adhesion of atoms, ions, bimolecules or molecules of gas, liquid or dissolved solids to a surface is called adsorption. In this process creates a film of the adsorbate –the molecules or atoms being accumulated, on the surface of the adsorbent. In absorption, the molecules of a substance are uniformly distributed in the bulk of the other, whereas in adsorption molecules of one substance are present in higher concentration at the surface of the other substance. Depending upon the nature of forces existing between adsorbate molecules and adsorbent, the adsorption can be classified into two types:

✓ Physical adsorption (physisorption): If the force of attraction existing between adsorbate and adsorbent are Vander Waal's forces, the adsorption is called physical adsorption. It is also known as Vander Waal's adsorption. In physical adsorption the force of attraction between the adsorbate and adsorbent are very weak, therefore this type of adsorption can be easily reversed by heating or by decreasing the pressure.

✓ Chemical adsorption (chemisorption): If the force of attraction existing between adsorbate and adsorbent are almost same strength as chemical bonds, the adsorption is called chemical adsorption. It is also known as Langmuir adsorption. In chemisorption the force of attraction is very strong, therefore adsorption cannot be easily reversed.

Attempts were made to fit values of  $\theta$  to many isotherm including Langmuir, Temkin Frumkin and Freundlich. The organic compound seems that follows well the Langmuir adsorption isotherm. The Langmuir equation (also known as the Langmuir isotherm, Langmuir adsorption equation or Hill-Langmuir equation) relates the coverage or adsorption of molecules on a solid surface to gas pressure or concentration of a medium above the solid surface at a fixed temperature. The equation was developed by Irving Langmuir in 1916 [22]. The equation is stated as

$$\frac{C}{\theta} = \frac{1}{K} + C \quad (15)$$

$$K = \frac{1}{55.5} \exp\left(-\frac{\Delta G_{ads}^{\circ}}{RT}\right) \quad (16)$$

where  $C$  is the concentration of inhibitor,  $K$  is the adsorptive equilibrium constant,  $\theta$  is the surface coverage and the standard adsorption free energy ( $\Delta G_{ads}$ ).

Langmuir isotherm can also be derived using statistical mechanics with the following assumptions:

- Suppose there are  $M$  active sites to which  $N$  particles bind.
- An active site can be occupied only by one particle.
- Active sites are independent. Probability of one site being occupied is not dependent on the status of adjacent sites.

The relationship between  $C/\theta$  and  $C$  presents linear behaviour at all temperatures studied (Fig. 4 and 5) with slopes equal to unity.

To get more adsorption enthalpy,  $\Delta H_{ads}^{\circ}$ , the Van't Hoff equation was used [23]:

$$\ln(K) = -\frac{\Delta H_{ads}^{\circ}}{RT} + Constant \quad (17)$$

The straight line obtained between  $\ln(K)$  and  $1/T$  leads to  $\Delta H^\circ_{ads} = -44.26 \text{ kJ.mol}^{-1}$  which is equal to that estimated by the Gibbs–Helmholtz equation, expressed by:

$$\left[ \frac{\partial(\Delta G^\circ_{ads}/T)}{\partial T} \right]_P = -\frac{\Delta H^\circ_{ads}}{T^2} \tag{18}$$

and written in the following equation.

$$\frac{\Delta G^\circ_{ads}}{T} = \frac{\Delta H^\circ_{ads}}{T} + A \tag{19}$$

The standard adsorption entropy  $\Delta S^\circ_{ads}$  may be deduced using the thermodynamic basic equation:

$$\Delta G^\circ_{ads} = \Delta H^\circ_{ads} - T\Delta S^\circ_{ads} \tag{20}$$

All the obtained thermodynamic parameters are shown in Table 6. The negative values of  $\Delta G^\circ_{ads}$  for P1 indicate the spontaneous of the adsorption of P1 and stability of the adsorbed layer on the steel surface. More negative value designates that inhibitor is strongly adsorbed on the steel surface.

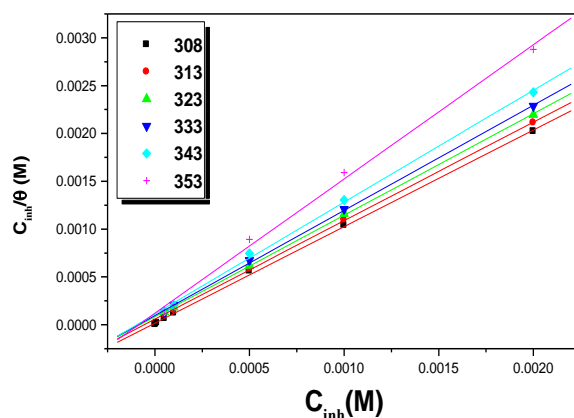


Figure 4. The relation between  $C/\theta$  and  $C$  of P1 at various temperatures

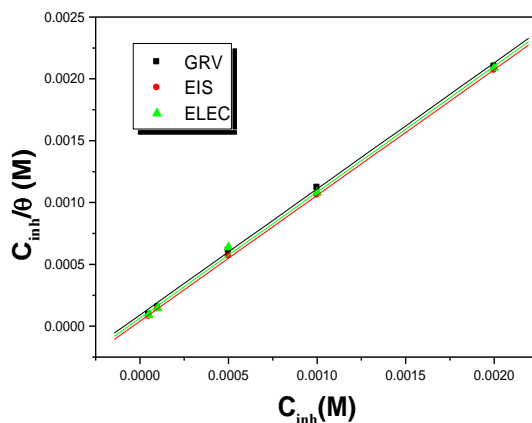
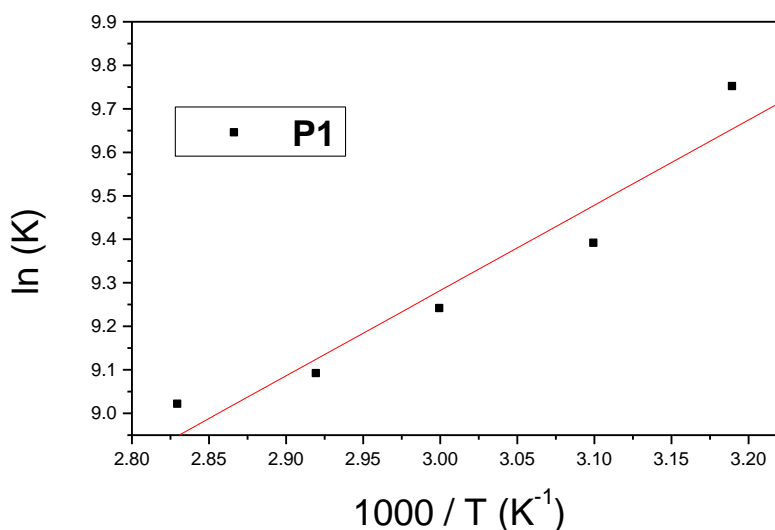


Figure 5. Langmuir isotherm of steel in the 1M HCl in presence of P1 at calculated by various method.

The negative values of  $\Delta H^{\circ}_{ads}$  also show that the adsorption of inhibitor is an exothermic process [19]. It assumed that an exothermic process is attributed to either physical or chemical adsorption but endothermic process corresponds solely to chemisorption. In an exothermic process, physisorption is distinguished from chemisorption by considering the absolute value of a physisorption process is lower than  $20 \text{ kJ mol}^{-1}$  while the adsorption heat of a chemisorption process approaches  $100 \text{ kJ mol}^{-1}$  [20].

In this study; the standard adsorption heat  $-35.81 \text{ kJmol}^{-1}$  postulates that a physical adsorption is more favoured. The negative values of  $\Delta S^{\circ}_{ads}$  is generally explained an ordered of adsorbed molecules of inhibitor with the progress in the adsorption onto the steel surface [24].

Literature pointed that values of  $\Delta G^{\circ}_{ads}$  around  $-20 \text{ kJ.mol}^{-1}$  or lower are related to the electrostatic interaction between the charged molecules and the charged metal (physisorption); those around  $-40 \text{ kJ.mol}^{-1}$  or higher involve charge sharing or transfer from organic molecules to the metal surface to form a coordinate type of bond (chemisorption) [19]. The obtained values of  $\Delta G^{\circ}_{ads}$  from  $-35.81$  to  $38.23 \text{ kJ.mol}^{-1}$  at different temperature, indicating, that the adsorption mechanism of the P1 on steel in 1M HCl solution is attributed to either physical or chemical adsorption (Table 6).



**Figure 6.** The relationship between  $\ln(K)$  and  $1/T$  for P1

**Table 6.** Thermodynamic parameter of adsorption of P1 at different temperature

T(k)	R	K	$\Delta G^{\circ}_{ads}$ (kJ.mol <sup>-1</sup> )	$\Delta H^{\circ}_{ads}$ (kJ.mol <sup>-1</sup> )	$\Delta S^{\circ}_{ads}$ (J.mol <sup>-1</sup> .K <sup>-1</sup> )
308	0.99965	$5.67 \cdot 10^4$	-38.30	-16.29	71.45
313	0.99995	$1.71 \cdot 10^4$	-35.81		62.36
323	0.99992	$1.19 \cdot 10^4$	-35.98		60.95
333	0.99979	$1.03 \cdot 10^4$	-36.68		61.24
343	0.99933	$8.89 \cdot 10^3$	-37.37		61.45
353	0.99847	$8.23 \cdot 10^3$	-38.23		62.15

The variation of  $\Delta G^{\circ}_{ads}/T$  with  $1/T$  gives a straight line with a slope that equals  $\Delta H_{ads} = -16.29$  kJ/mol. It can be seen from the Fig6. That  $\ln(K)$  increases with  $1/T$  in a linear for P1.

### 3.3. Polarisation curves

Electrochemical polarization curves for steel in synthetic solution at different concentrations are plotted in Fig. 7, shows the cathodic and anodic polarisation curves of iron in 1M HCl in the absence and presence of (E)-4-methoxy-N-(methoxybenzylidene)aniline (P1) and (E)-N-(4-methoxybenzylidene)-4-nitroaniline (P2) at various concentrations. Table 7 reports the electrochemical parameters such as the corrosion potential ( $E_{corr}$ ), the corrosion current density ( $I_{corr}$ ) determined by extrapolation of cathodic Tafel lines to the corrosion potential ( $E_{corr}$ ), the cathodic Tafel slope ( $\beta_c$ ) and resistance of polarisation ( $R_p$ ).

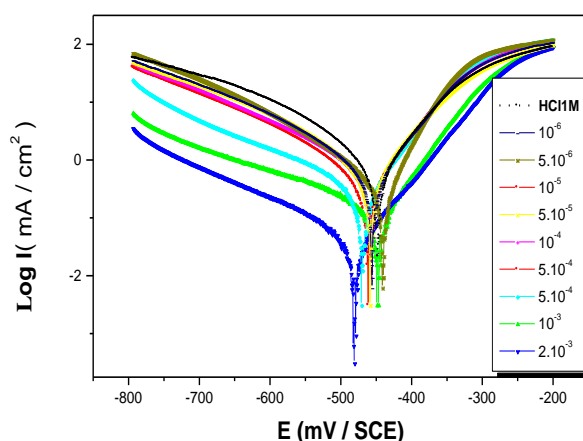


**Figure 7.** Cathodic and anodic plots for steel with P1 at various concentrations

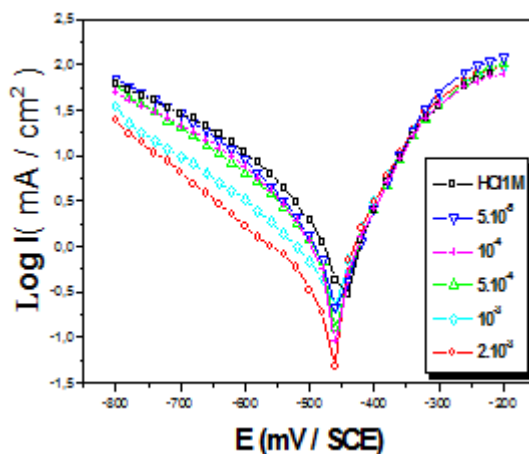


**Figure 8.** Cathodic and anodic plots for steel with P2 at various concentrations

As can be seen from this Fig.7; the addition of the P1 and P2 decreases the corrosion current density, (Fig.7 and Table 7). The cathodic portions rise to Tafel lines indicating that the hydrogen evolution reaction was activation controlled. The addition of the compounds to the corrosive solution does not modify the mechanism of the reduction processes. The free corrosion potentials determined after one hour of immersion are slightly modified in the presence of the inhibitor. E% increases with the concentration of P1 and attains a maximum value of 96 % at  $10^{-6}$  M. The P1 is then an excellent inhibitor than P2. From the anodic curves we deduce that P1 acts as a mixed-type inhibitor Fig. 7; but P2 act essentially a cathodic type inhibitor Fig. 8.

**Table 7.** Electrochemical parameters for iron in 1M HCl at various concentrations of P1 and P2.

Inhibitors	Concentration (M)	E <sub>corr</sub> (mV/ECS)	$-\beta_c$ (mV/dec)	$\beta_a$ (mV/dec)	R <sub>p</sub>	I <sub>corr</sub> ( $\mu\text{A}/\text{cm}^2$ )	E <sub>1</sub> %	E <sub>Rp</sub> %
HCl	1	-448	124	71	30	540	--	--
P1	$10^{-6}$	-459	136	74	32	458	15.19	6.25
	$5.10^{-6}$	-457	130	66	35	391	27.59	14.29
	$10^{-5}$	-442	132	59	49	338	37.41	38.78
	$5.10^{-5}$	-462	138	67	50	300	44.44	40.00
	$10^{-4}$	-452	174	58	115	127	76.48	73.91
	$5.10^{-4}$	-449	194	59	160	84	84.44	81.25
	$10^{-3}$	-402	166	66	233	70	87.04	87.12
	$2.10^{-3}$	-509	156	95	857	26	95.19	96.50
P2	$5.10^{-5}$	-452	118	69	35	453.5	16.02	15.04
	$10^{-4}$	-402	182	73	40	402.5	25.46	25.63
	$5.10^{-4}$	-457	118	70	46	324.9	39.83	35.46
	$10^{-3}$	-477	149	75	50	313	42.04	39.87
	$2.10^{-3}$	-442	126	70	91	205.5	61.94	67.04

### 3.4. Electrochemical impedance spectroscopy (EIS)

EIS is carried out by imposing potential sweeps, potential steps, or current steps, we typically drive the electrode to a condition far from equilibrium, and we observe the response, which is usually a transient signal. Another approach is to perturb the cell with an alternating signal of small magnitude and to observe the way in which the system follows the perturbation at steady state. Many advantages accrue to these techniques. This measurement is equivalent to determining the faradic impedance. EIS is essentially a steady state technique that is capable of accessing relaxation phenomena whose relaxation times vary over orders of magnitudes and permits single averaging within a single experiment to obtain high precision levels. It confirms the conventional polarization techniques for corrosion rate measurements. The technique has been widely used in investigating corrosion inhibition processes. It also provides information on both the resistive and capacitive behaviour at interface and makes possible to evaluate the performance of the tested compounds as possible inhibitors against metal corrosion [19].

Electrochemical impedance spectroscopy (EIS) measurements have been carried out at 308 K in acidic solution with and without P1 compound (Fig 9) and P2 Fig.10. The charge-transfer resistance

( $R_t$ ) values are calculated from the difference in impedance at lower and higher frequencies. The double layer capacitance ( $C_{dl}$ ) and the frequency at which the imaginary component of the impedance is maximal ( $-Z_{max}$ ) are found as represented in equation:

$$C_{dl} = \left( \frac{1}{\omega \cdot R_t} \right) \quad \text{where} \quad \omega = 2\pi f_{max} \tag{21}$$

The inhibition efficiency got from the charge transfer resistance is calculated by:

$$E_Z (\%) = 100 \cdot ( 1 - R_t / R_{t/inh} ) \tag{22}$$

$R_t$  and  $R_{t/inh}$  are the charge transfer-resistance values without and with inhibitor, respectively.

The impedance diagram obtained with 1 M HCl shows only one depressed capacitive loop at the higher frequency range. The same trend was also noticed for C38 steel immersed in 1 M HCl containing P1 and P2. In Table 9, impedance parameters of the Nyquist plots of the P1 and P2 in different concentrations are given.  $R_t$  is a measure of electron transfer across the surface and is inversely proportional to corrosion rate.

The most common equivalent circuit used to model corrosion of C-steel in aqueous acidic solution is the Randles circuit. The HF capacitive loop could be attributed to the double layer capacity in parallel with the charge-transfer resistance ( $R_t$ ) (Fig. 9 and 10). The constant phase element, CPE, is introduced in the circuit instead of a pure double layer capacitor to give a more accurate fit [19]. The diameter of Nyquist plots increases on increasing the P1 concentration. This suggested that the formed inhibitive film was strengthened by addition of P1. Besides, the presence of low frequency (LF) inductive may be attributed to the relaxation process obtained by adsorption species like  $Cl_{ads}^{-1}$  and  $H_{ads}^{+}$  on the electrode surface.

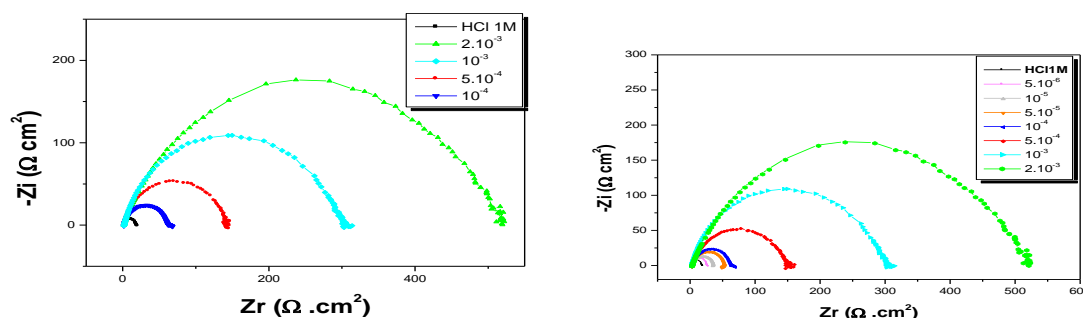


Figure 9. Impedance parameters for Steel in 1M HCl for various concentrations of P1.

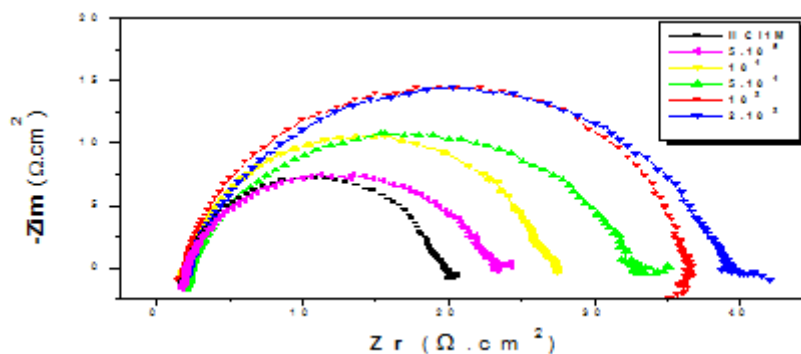


Figure 10. Impedance parameters for Steel in 1M HCl for various concentrations of P2

It should be noted that a CPE could be treated as a parallel combination of a pure capacitor and a resistor being inversely proportional to the angular frequency. The CPE, which is considered a surface irregularity of the electrode, causes a greater depression in Nyquist semicircle diagram, where the metal–solution interface acts as a capacitor with irregular surface.

Electrical equivalent circuits are generally used to model the electrochemical behaviour and to compute the parameters of interest. When there is non-ideal frequency response, it is common practice to use distributed circuits elements in the equivalent circuit (Fig. 11 and table 8). The most widely used is the constant phase element (CPE) which has a non-integer power dependence on the frequency.

In most times, CPE is required for modelling the frequency dispersion behaviour corresponding to different physical phenomena such as surface heterogeneity which results from surface roughness, impurities, dislocations, distribution of the active sites, adsorption of inhibitors and formation of porous layer.

As it can be seen from Table 9, the  $R_1$  values increased with the increasing the concentrations of the inhibitors. On the other hand, the values of  $C_{dl}$  decreased with an increase in the inhibitors concentration thus with inhibition efficiencies. This situation was the result of an increase the surface coverage by the inhibitor, which led to an increase in the inhibition efficiency. This decrease in the  $C_{dl}$  can result from a decrease in local dielectric constant and/or an increase in the thickness of the electrical double layer, signifying that molecule inhibitors acts by adsorption at the solution/interface .

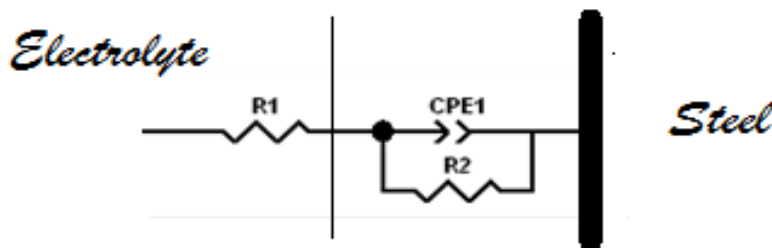


**Figure 11.** Electrochemical equivalent circuit diagram for metal–electrolyte interface.

**Table 8.** Value of equivalent circuit elements of P1 at maximum concentration.

Circuit elements	Value	Error
R1	2034	$6.0669 \cdot 10^{-5}$
CPE1-T	$1.6792 \cdot 10^{-5}$	$6.09 \cdot 10^{-20}$
CPE-P	0.82486	$4.06 \cdot 10^{-16}$
R2	859.4	$8.27 \cdot 10^{-13}$

**Table 9.** Impedance parameters for steel in 1M HCl at various concentrations of P1 and P2.

	Concentration (M)	$R_s$ ( $\Omega \cdot \text{cm}^2$ )	$R_t$ ( $\Omega \cdot \text{cm}^2$ )	f (Hz)	$C_{dl}$ ( $\mu\text{F}/\text{cm}^2$ )	E (%)
Blank	1	2.069	17,71	125,07	71,89	---
P1	$10^{-6}$	1.800	19.00	120.00	69.28	06.79
	$5 \cdot 10^{-6}$	1.850	26.00	98.00	62.18	31.85
	$10^{-5}$	2.360	31.00	90.00	57.00	42.81
	$5 \cdot 10^{-5}$	1.980	49.00	79,10	41,08	63.80
	$10^{-4}$	1.734	62.00	78,83	32,58	71.37
	$5 \cdot 10^{-4}$	1.809	148.0	60,61	17,75	88.00
	$10^{-3}$	0.860	301.0	40,10	13,19	94.10
	$2 \cdot 10^{-3}$	0.508	517.0	31,71	09,71	96.56
P2	$10^{-5}$	2.060	21.20	2330.21	70.01	16.46
	$5 \cdot 10^{-5}$	2.060	25.00	2717.28	69.23	29.16
	$10^{-4}$	2.350	30.72	3074.21	63.74	42.35
	$5 \cdot 10^{-4}$	1.980	34.31	3147.43	58.43	48.38
	$10^{-3}$	2.140	37.18	3890.46	49.56	52.37

The impedance spectra for P1 and P2 obtained on iron in 1 M HCl solutions consist of one depressed capacitive loop (one time constant in the Bode-phase representation (Fig. 9 and 10). When Nyquist plot contains a “depressed semicircle with the center under the real axis, such behavior is characteristic for solid electrodes and often referred to as frequency dispersion has been attributed to roughness and other inhomogeneities of the solid surface [19].

In these cases the parallel network charge transfer resistance double layer capacitance ( $R_t/C_{dl}$ ) - is usually a poor approximation especially for systems where an efficient inhibitor is present. For the description of a frequency independent phase shifts between an applied AC potential and its current response.

### 3.5. Quantum chemical investigation

Quantum chemical approach, using the density functional theory (DFT), was applied in order to get better understanding about the relationship between the inhibition efficiency and molecular structure of **P1** and **P2**. The calculated quantum chemical parameters include the highest occupied molecular orbital (HOMO), lowest unoccupied molecular orbital (LUMO), dipole moment and amount of electrons transferred. The results of the study suggest that P1 is a better corrosion inhibitor than P2, which is in agreement with most experimental findings obtained at different concentrations [11, 12].

All geometry optimizations and quantum chemical calculations were performed using density functional theory (DFT) because it is a trade-off between computational cost, the complexity of the inhibitors studied, the selected molecular properties to be calculated and reasonability of the desired results [8]. .

**Table 10.** Quantum parameters of P1 and P2

Inhibitors	P1	P2
1N	-0.150344	-0.151603
2C	-0.047641	-0.014245
3C	-0.121702	-0.076985
4C	-0.150492	-0.096137
5C	0.078339	-0.005355
6C	-0.202524	-0.149101
7C	-0.066710	-0.141840
8C	-0.009866	0.175965
9C	-0.104152	-0.283984
10C	-0.052719	-0.214658
11C	-0.169158	-0.018199
12C	0.095538	-0.082939
13C	-0.213763	-0.097411
14C	-0.073281	-0.155281
15O	-0.207736	0.046385
16C	-0.077096	-0.152278
17C	-0.209543	-0.057281
18C	-0.076422	-0.205620

The Becke's Three Parameter Hybrid Functional using the Lee-Yang-Parr correlation functional theory (B3LYP, [1]) was selected for the calculations. Calculations were done with the 6-31+G(d,p) basis set. The addition of diffuse functions is considered important for a good description of ionic systems [2]. Among the molecular properties calculated include the electronegativity, chemical hardness and chemical softness. Electronegativity ( $\chi$ ) is the measure of the power of an electron or group of atoms to attract electrons towards itself [3] and according to Koopman's theorem [4, 5] it can be estimated by using the following equation:

$$\chi \cong -\frac{1}{2} (E_{\text{HOMO}} + E_{\text{LUMO}}) \quad (23)$$

Chemical hardness ( $\eta$ ) measures the resistance of an atom to a charge transfer [6], it is estimated by using the equation:

$$\eta \cong -\frac{1}{2} (E_{\text{HOMO}} - E_{\text{LUMO}}) \quad (24)$$

Electron polarizability, also called chemical softness ( $\sigma$ ), describes the capacity of an atom or group of atoms to receive electrons [6], it is estimated by using the equation:

$$\sigma = 1/\eta \cong -2/(E_{\text{HOMO}} - E_{\text{LUMO}}) \quad (25)$$

All calculations were done by using the Gausse03 program [7].

The substitute effect on the steel inhibition of the P1 and P2 will be rationalized using global reactivity indexes, namely, Mullikan charge are given in Tables 10

The theoretical calculation of the total partial charge density of heteroatom's in P1 and P2 molecular structures, can reinforce the suggestion that the inhibitory effect contributed by the groups constituting the rigid centre of the molecule and its adsorption to the surface of the mild steel. This distribution thus ensures strong adsorption onto the metal surface. The inhibitory action of these inhibitors depends on the concentration and the position of the nitrogen and oxygen atoms.

The optimized geometries, the HOMO density and the LUMO density for the inhibitors are shown in Fig. 12. Table 12 reports the molecular properties of interest, including the energy of the HOMO ( $E_{\text{HOMO}}$ ), energy of the LUMO ( $E_{\text{LUMO}}$ ), the dipole moment, chemical hardness and softness parameters. According to the frontier molecular orbital theory, chemical reactivity is strongly determined by the interaction of the highest occupied molecular orbital (HOMO) and the lowest unoccupied molecular orbital (LUMO) of the interacting species [8]. In P1, the HOMO is strongly dominated by the HOMO of the inhibitors; in P1, the HOMO is substitution on the  $\text{OCH}_3$  functional group of the P1 by NOO functional group of the P2. The LUMO on both structures is localized on the rings.

The frontier molecular orbital energies (i.e.,  $E_{\text{HOMO}}$  and  $E_{\text{LUMO}}$ ) provide information on the reactivity of chemical species. The  $E_{\text{HOMO}}$  is often associated with the electron donating ability of a molecule [9–11] and a higher  $E_{\text{HOMO}}$  energy value indicates higher tendency of the molecule to donate electron(s) to the appropriate acceptor molecule with low energy and empty/partially filled molecular orbital. This implies that molecules with high values of  $E_{\text{HOMO}}$  have a greater tendency to adsorb (and therefore greater inhibition efficiency) on the surface of the metal. The results reported in table 12 show that  $E_{\text{HOMO}}$  for P1 is higher than that of P2, suggesting that P1 has the highest tendency to donate electrons to the surface of the metal and therefore would have the highest adsorption, leading to greatest inhibition efficiency.

The  $E_{\text{LUMO}}$  indicates the ability of the molecule to accept electrons and the lower the value of  $E_{\text{LUMO}}$  the easier it is that the molecule would accept electrons [9]. The results reported in table 12 show that the  $E_{\text{LUMO}}$  is lowest for P1 and highest for P2, what suggest that P1 would readily accept electrons from the metal.

Molecules with large value of  $\Delta E$  are highly stable (i.e., they have low reactivity to chemical species) while molecules with small values of  $\Delta E$  have a high reactivity. A molecule with a small value of  $\Delta E$  is easily polarized and can therefore be easily adsorbed on the metal surface, resulting in appreciably good inhibition efficiency. The data reported in table 12 show that P2 has the smallest  $\Delta E$  value.

Absolute hardness ( $\eta$ ) and softness ( $\sigma$ ) are properties that also facilitates the analysis of the molecular reactivity and selectivity. The relationship between these quantum chemical quantities and corrosion inhibition is often based on the Lewis theory of acid and bases and Pearson's hard and soft acids and bases [12]. A hard molecule has a large  $\Delta E$  while a soft molecule has a small  $\Delta E$ . Soft molecules therefore could easily offer electrons to an acceptor system what makes them more reactive than hard molecules. In this regard, adsorption could occur at the region of the molecule where  $\sigma$  has the highest value [13]. The values of  $\sigma$  reported in table 12 show that P2 has the highest  $\sigma$  value and would therefore be expected to have the highest % inhibition efficiency.

The number of transferred electrons ( $\Delta N$ ) represents the fraction of electrons transferred from the donor to the acceptor molecule (in this case from the inhibitor to the mild steel surface) and it is estimated following the equation [14–16]:

$$\Delta N = \chi_{\text{Fe}} - \chi_{\text{inh}} / 2(\eta_{\text{Fe}} - \eta_{\text{inh}}) \quad (26)$$

where  $\chi_{\text{Fe}}$  and  $\chi_{\text{inh}}$  denote the absolute electronegativity of iron and the inhibitor molecule respectively;  $\eta_{\text{Fe}}$  and  $\eta_{\text{inh}}$  denote the absolute hardness of iron and the inhibitor molecule respectively.

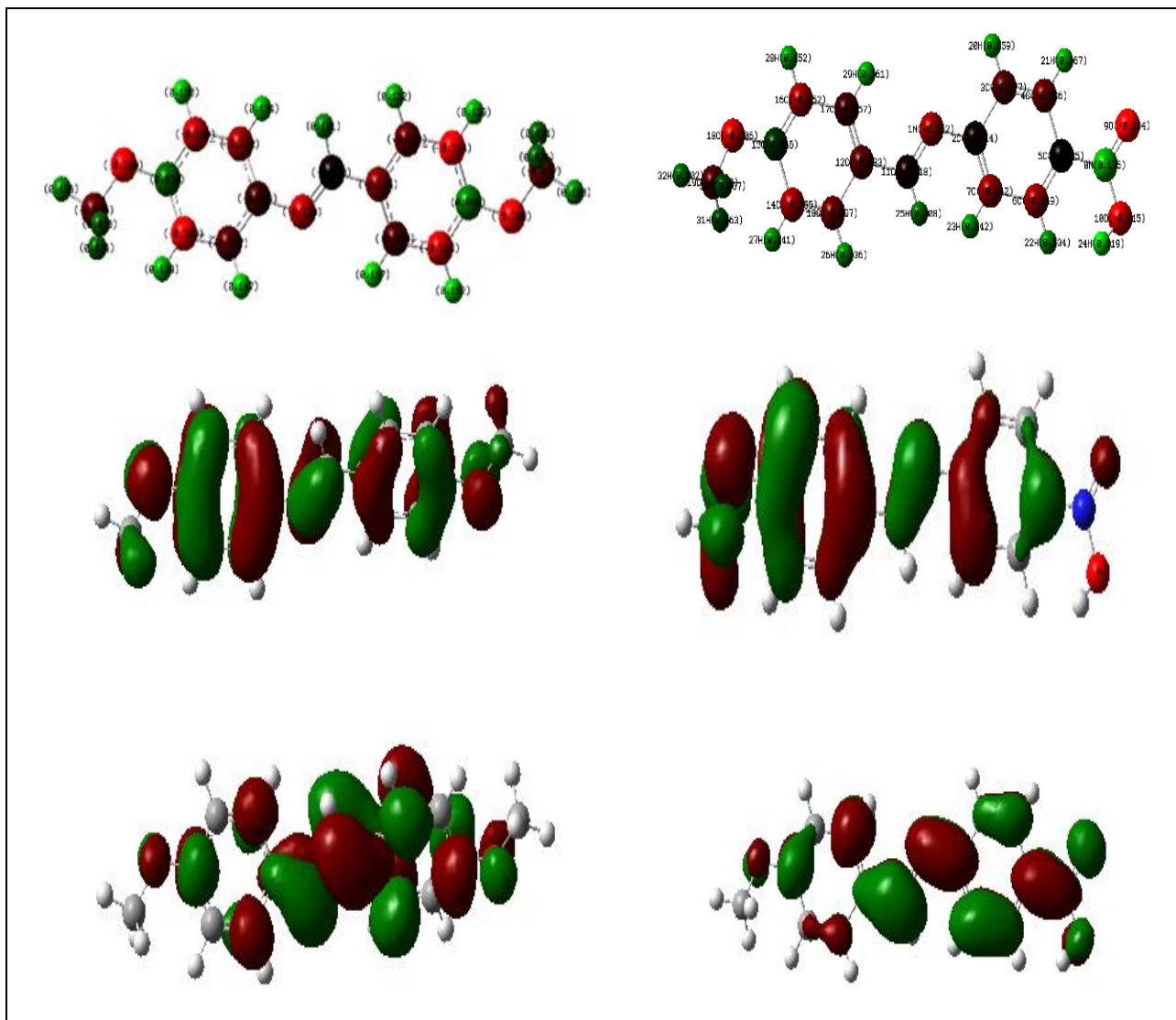


**Figure 12.** The optimized structures, the HOMO densities and the LUMO densities for the studied ionic liquid, results with B3LYP/6-31+G(d,p) method.

The values of  $\chi_{\text{Fe}}$  and  $\eta_{\text{Fe}}$  are taken as  $7 \text{ eVmol}^{-1}$  and  $0 \text{ eVmol}^{-1}$  respectively [16, 17]. The results are reported in table 12 and show that all the inhibitors have negative  $\Delta N$  values; P1 has the highest  $\Delta N$  value, corresponding to highest inhibition efficiency. Following the study in [18], where it was observed that for  $\Delta N < 3.6$ , the inhibition efficiency increases with electron donating ability at the metal surface, it is reasonable to infer that P1 has the highest electron-donating ability and has the highest inhibition efficiency.

The dipole moment ( $\mu$ ) is another index that is often used for the prediction of the direction of a corrosion inhibition process. It is the measure of polarity in a bond and is related to the distribution of electrons in a molecule [19]. Inhibitors with high dipole moment tend to form strong dipole-dipole interactions with the metal, resulting in strong adsorption on the surface of the metal and therefore leading to greater inhibition efficiency [20, 23]. However, a survey of literature shows that in most cases, experimental inhibition efficiencies do not always correlate with dipole moments [24]. The results reported in table 12 show that P1 has the smallest dipole moment value

We have demonstrated that there is a systematic change of the HOMO and LUMO energies into the backbone causing a destabilization for HOMO and LUMO levels and lowering the energy band gap. On the other hand, it will be useful to examine the HOMO and the LUMO for these studied molecules because the relative ordering of occupied and virtual orbital provides a reasonable qualitative indication of excitation properties and provides also the ability of electron hole transport. In general, and as plotted in Fig. 12, (LUMO, HOMO); the HOMO possesses an anti-bonding character between the consecutive subunits. On the other hand, the LUMO of all studied compounds generally shows a bonding character between the subunits where a theoretical value for the electronegativity of bulk iron was used,  $\chi_{\text{Fe}} = 7 \text{ eV}$ , and a global hardness of  $\eta_{\text{Fe}} = 0$  was used.

**Table 12.** Calculated quantum chemical parameters of the studied compounds.

Quantum parameters	P1	P2
$E_{\text{HOMO}}$ (eV)	-0.206	-0.321
$E_{\text{LUMO}}$ (eV)	-0.307	-0.218
$\Delta E_{\text{gap}}$ (eV)	0.101	0.103
$\mu$ (debye)	1,627	5.9188
$I = -E_{\text{HOMO}}$ (eV)	0.206	0.321
$A = -E_{\text{LUMO}}$ (eV)	0.307	0.218
$\chi = (I+A)/2$ (eV)	0.256	0.2695
$\eta = (I-A)/2$ (eV)	-0.153	0.0515
$\sigma = 1/\eta$	-6.535	19.4175
$\omega = \mu/2\eta$	-5.316	0.15241
$\Delta N = (\chi_{\text{Fe}} - \chi_{\text{inh}})/2(\eta_{\text{Fe}} - \eta_{\text{inh}})$	-0.515	-0.17331
TE(u.a.)	-0.00432377	0.17686362

#### 4. CONCLUSION

The principal finding of the present work can be summarised as follows:

- Steady state electrochemical measurements have shown that the P1 acts a mixed type inhibitors and the P2 acts predominantly as a cathodic inhibitor for the corrosion of steel in 1M HCL without modifying the mechanism of hydrogen evolution reaction.
- The polarization resistance of the system increases when the inhibitor is added to the solution.
- The adsorption of the P1 and P2 on the steel surface in 1M HCl obeys to the Langmuir adsorption isotherm model.
- The inhibition efficiency of P1 increases with the temperature and the activation corrosion energy decreases in presence of inhibitor.
- Quantum chemical studies have been performed, using the B3LYP/6-31+G(d,p) method to investigate the properties of two newly synthesized inhibitors and how their molecular properties relate to their ability to inhibit metal corrosion. A comparison of all the molecular properties suggests that P1 is a better corrosion inhibitor than P2.

## ACKNOWLEDGEMENTS

The Authors extend their appreciation to the Deanship of Scientific Research at King Saud University for funding the work through the research group project No. RGP-089

## Reference

1. P. Mohan, R. Usha, G.P. Kalaignan, V.S. Muralidharan, *J. Chem* (2013).
2. R. Arefinia, A. Shojaei, H. Shariatpanahi, J. Neshati, *Prog. Org. Coat*, 75 (2012) 502.
3. S. Ahmad, F. Zafar, E. Sharmin, N. Garg, M. Kashif, *Prog. Org. Coat*, 73 (2012) 112.
4. M. Abdallah, I. Zaaferany, K.S. Khairou, Y. Emad, *Chem. Tech. Fuels and Oils*, 48 (2012) 234.
5. W. Chen, H.Q. Luo, N.B. Li, *Corros. Sci*, 53 (2011) 3356.
6. H. Akrouf, L. Bousselemi, S. Maximovitch, E. Triki, F. Dalard, *J. Mat. Sci*, 47 (2012) 8085.
7. A. Chetouani, A. Aouniti, B. Hammouti, N. Benchat, T. Benhadda, S. Kertit, *Corros. Sci*, 45 (2003) 1675.
8. E.H. El Ashry, A. El Nemr, S. Ragab, *J. Mol. Modeling*, 18 (2012) 1173.
9. L.T. Sein, *J. Mol. Str.*, 1000 (2011) 109.
10. K. Laarej, M. Bouachrine, S. Radi, S. Kertit, B. Hammouti, *E-J. Chem*, 7 (2010) 419.
11. M. Bouklah, H. Harek, R. Touzani, B. Hammouti, Y. Harek, *Arab. J. Chem*, 5 (2012) 163.
12. N. Boussalah, S. Ghalem, S. El Kadiri, B. Hammouti, R. Touzani, *Res. Chem. Inter*, 38 (2012) 2009.
13. P. Udhayakala, T. V. Rajendiran, S. Gunasekaran, *Journal of Computational Methods in Molecular Design*, 2 (1) (2012) 1.
14. A. Kokalj, *Chemical Physics*, 393 (2012) 1.
15. X.M. Wang, H.Y. Yang, F.H. Wang, *Corros. Sci*, 55 (2012) 145.
16. A. Kokalj, N. Kovacevic, S. Peljhan, M. Finsgar, A. Lesar, I. Milosev, *Chemphyschem*, 12 (2011) 3547.
17. M. Abdallah, I. Zaaferany, A.S. Fouda, D. Abd El-Kader, *J. Mat. Eng. Perf*, 21 (2012) 995.
18. J.K. Sahu, K.K. Sahu, A.K. Ray, Proceedings of the Institution of Mechanical Engineers Part L-J. *Mat.-Design and Appl*, 226 (2012) 34.
19. A. Chetouani, M. Daoudi, B. Hammouti, T. Ben Hadda, M. Benkaddour, *Corros. Sci*, 48 (2006) 2987.
20. A. Chetouani, B. Hammouti, T. Benhadda, M. Daoudi, *Appl. Surf. Sci*, 249 (2005) 375.
21. S. Kertit, B. Hammouti. *Appl. Surf. Sci*. 93 (1996) 59.
22. I. Langmuir, *Journal American Chemical Society*, 38 (1916) 2221
23. I M. Bouklah, N. Benchat, B. Hammouti, S. Kertit, *Mater. Let*. 60 (2006) 1901
24. M.J. Firdhouse, D. Nalini, *J. Chem*. (2013) Art. no. 835365.